JOURNAL OF MATERIALS SCIENCE 23 (1988) 4144–4156

Deformation mechanisms in yttria-stabilized zirconia

J. LANKFORD, R. A. PAGE
Department of Materials Sciences, Southwest Research Institute, San Antonio, Texas, USA
L. RABENBERG
Department of Mechanical Engineering and Center for Materials Science and Engineering, University of Texas, Austin, Texas, USA

Yielding behaviour and deformation modes are characterized for single-crystal and polycrystalline yttria-stabilized ZrO_2 tested in compression from 23 to 800° C. The plastic flow of single-crystal specimens is shown to be orientation and temperature dependent, and is interpreted in terms of dislocation activity, transformation plasticity, and ferroelastic domain switching. Polycrystalline material deforms at room temperature by transformation plasticity, and at intermediate temperatures ($\sim$ 800° C) by forming unstable shear bands, which flow via grain-boundary sliding and cavitation.

1. Introduction

Zirconia-based ceramics stabilized with yttria to provide high-volume fractions of the tetragonal phase have recently been shown to exhibit extremely attractive mechanical properties. For example, researchers have reported flexural strengths as high as 2 GPa [1], and fracture toughnesses approaching 10 MPa $m^{1/2}$ [2]. Unfortunately, these results obtain only near room temperature; as the temperature is raised, both strength and toughness decline. This loss in toughness is generally attributed to diminution in the effectiveness of the tetragonal-to-monoclinic transformation as a source of inelastic strain. The latter can lead to toughening in a variety of distinct ways, as reviewed by Evans and Cannon [1].

On the other hand, the very mechanisms of plasticity which enhance toughness in zirconia appear ultimately to be strength limiting [3, 4]. In particular, the toughening mechanisms generally manifest themselves as microstructurally localized shear bands, produced by a cooperative precipitate transformation process documented most extensively for MgO-stabilized PSZ. Chen and Reyes-Morel [3] have recently shown that for the latter material, shear localization due to martensitic transformation plasticity is a principal source of microfracture, specifically at the intersections of shear bands and grain boundaries. These microfracture ensembles, rather than conventional intrinsic processing defects such as pores, are then responsible for failure via crack coalescence and/or growth.

At present, the role of transformation plasticity in the development of damage in yttria-stabilized zirconia (yttria–tetragonal zirconia polycrystals (Y-TZP) and yttria-partially stabilized zirconia (Y-PSZ)) has seen only limited study. This, despite the fact that some Y-TZP systems exhibit the extremely high strength/high toughness combination cited above, and that phase transformations in Y-PSZ differ considerably from those in Mg-PSZ [5]. An experimental study of deformation and damage mechanisms in these systems is clearly desirable.

The present work represents an effort in this direction, but one which is compromised by the nature of the available ZrO_2 microstructures. Specifically, polycrystalline PSZ, which can be stabilized with any of several elements (such as magnesium and calcium), usually consists of fairly large cubic grains, within each of which is a high density of small, metastable tetragonal precipitates. On the other hand, TZP (stabilized by cerium or yttrium) is composed essentially of fine, wholly tetragonal (t) grains. These may either transform to the monoclinic (m) phase or, based on recent experiments by Virkar and Matsumoto [6], undergo a stress-induced ferroelastic domain reorientation, whereby an *a*-axis stretches into a *c*-axis, and correspondingly the *c*-axis becomes an *a*-axis. It also is possible for these two mechanisms to operate concurrently.

Polycrystalline PSZ and TZP are both characterized by continuous amorphous grain-boundary (GB) films [7, 8], added during processing as sintering aids and, for TZP, as a means of limiting grain growth. It is well known that in other non-transformable ceramic systems with glassy GB, elevated-temperature mechanical properties are degraded by GB sliding and creep cavitation within the glassy phase. This process has been briefly explored for Mg-PSZ [9], but has not yet been investigated for TZP.

In order to separate the various possible contributions of transcrystalline inelastic mechanisms (phase transformations, ferroelasticity, dislocation activity) from deformation caused by grain-boundary sliding, it would be desirable to compare the deformation behaviour of equivalent single crystal and polycrystal variants. However, currently available single crystals

0022–2461/88 $03.00 + .12

consist of either Y-PSZ or Y-fully stabilized cubic zirconia. Although Y-PSZ crystals are of interest in the present case, they are not analogous to Y-TZP (polycrystalline) material, i.e. a Y-PSZ crystal does not consist of a transformable tetragonal body. Instead, it is composed of either a cubic or "non-transformable" tetragonal [10] (t′) matrix phase containing a high density of relatively small, transformable tetragonal (t) precipitates. Thus, these crystals are more analogous to (Mg, Ca)-PSZ than they are to Y-TZP, hence their designation Y-PSZ.

Single crystals of Y-PSZ have interesting properties in their own right. While their low-temperature fracture toughness (9 to 10 MPa $m^{1/2}$) is thought to be due to the t → m transformation [1], their even greater toughness (~ 15 MPa $m^{1/2}$) at temperatures approaching 1500° C is probably caused by dislocation activity, as recently documented by Dominguez-Rodriguez *et al.* [11, 12].

Earlier, Lankford reported compressive deformation mechanisms in polycrystalline Mg-PSZ [9] and single crystal Y-PSZ crystals [13] oriented for single slip. The present report represents an extension of that work, and describes the results of a study of deformation, during compressive loading of Y-TZP and single crystal Y-PSZ oriented so as to activate multiple potential slip systems. In order to aid interpretation, the present results will be compared with those from earlier studies; a few key graphs and micrographs from the latter will be included and some earlier conclusions will be modified to reflect the new results reported here. Particular attention will be paid to behaviour in the temperature range 700 to 800° C, which represents the regime in which other mechanisms must begin to supercede the t → m transformation as the principal toughening mechanism.

2. Experimental procedures

Specimens for deformation experiments were fabricated from two types of yttria-stabilized ZrO_2. The first (Y-PSZ) consisted of a large 5 wt % Y_2O_3 zirconia single crystal (Ceres Corp., Waltham, MA, courtesy of R. P. Ingel, NRL, Washington, D.C.), which was oriented for sectioning using Laue X-ray diffraction. Cylindrical compression specimens 9 mm long × 4.5 mm diameter were machined from the parent crystal, with a ⟨1 0 0⟩ axial orientation relative to the tetragonal matrix. These crystals provided for multiple slip on either {1 1 1} ⟨1 $\bar{1}$ 0⟩ or {1 1 0} ⟨1 1 0⟩, with Schmid factors of 0.408 and 0.5, respectively. Earlier [13], nominally identical crystals were sectioned into specimens with ⟨1 2 3⟩ axial orientations, which corresponded to single slip on {0 0 1} ⟨1 1 0⟩. Specimen preparation procedures were identical to those used in the present work.

Based on the original characterization of similar crystals by Ingel [14], the microstructure of our as-received crystals was described in previous work [13] as a distribution of tetragonal precipitates coherent with a cubic matrix. Recent work by Lanteri *et al.* [10], however, has shown that the microstructure of these zirconia alloys may pass through several stages, of which cubic plus tetragonal is the final one depending on thermal history and alloy composition. Therefore, TEM was used to characterize the initial microstructure of our particular crystals. It was found that the single crystals consisted of three interlocking tetragonal variants of the metastable, diffusionless tetragonal, t′, phase. The three variants were arranged into equiaxed "colonies" of 0.5 μm typical size; within each colony, two variants with their *c*-axes 90° from each other formed alternating 80 nm bands, separated by planar, twin-related interfaces on {1 0 1} planes. Within the tetragonal variants, the transmission electron micrographs showed a mottled contrast due to overlapping strain fields of coherent precipitate particles. No chemical partitioning between t′ variants could be observed using energy dispersive spectroscopy in STEM; the precipitates within the t′ variants were too small to be resolved using this technique. It is believed that during slow cooling from the cubic phase during skull melting, coherent precipitation of yttria-poor tetragonal began, but was interrupted by the diffusionless transformation of the cubic matrix to the yttria-rich tetragonal phase.

Polycrystalline Y-TZP specimens were machined from as-received sintered material in the head-treated, partially stabilized condition (Norton YZ-110, Norton Co., Northborough, MA; characterized microstructurally by Ruhle *et al.* [7] as material number 11). Overall yttria content was roughly the same (5.8 wt %) as for the single crystals, but the actual Y_2O_3 concentrations within the grains differ significantly. In particular, Ruhle *et al.* [7] have shown that the preponderance of the grains are ~ 0.5 μm diameter tetragonal (t) phase, with an yttria composition of 3.0 to 4.1 wt %. The remainder of the material is composed of occasional Al_2O_3 grains, and cubic zirconia grains of the order of 0.6 to 2.0 μm diameter, with a Y_2O_3 composition of 6.7 to 9.4 wt %. All grain boundaries are covered by a ⩽ 10 μm thick amorphous grain-boundary phase, composed of Y_2O_3, SiO_2, Al_2O_3, and possibly ZrO_2 [7].

The polycrystalline Mg–PSZ (Nilsen TS-Grade PSZ; Nilsen Sintered Products, Ltd, Northcote, Victoria, Australia) studied earlier [9] was characterized by 60 μm cubic-phase grains containing a high density of roughly spherical small (0.05 to 0.1 μm) tetragonal (t) and monoclinic precipitates. Available evidence [8] indicates that Mg–PSZ, like Y-TZP, possesses a continuous GB film, composed primarily of SiO_2, CaO, and MgO.

Microstructural and ambient material properties for all three ZrO_2 variants studied are summarized in Table I.

Specimens were tested at temperatures ranging from 23 to 800° C, and at strain rates of 10^{-5} to 10^{-1} sec^{-1}. For elevated temperature testing, specimens were allowed to soak for 30 min in order to ensure that they were at equilibrium; it has been shown [15] that this period is insufficient to cause measurable loss of strength. Experiments required the use of ceramic loading platens, which were fabricated from high strength alumina; both specimens and platens were ground and lapped parallel to within 2 μm. Smooth (0.05 μm diamond) flats were polished

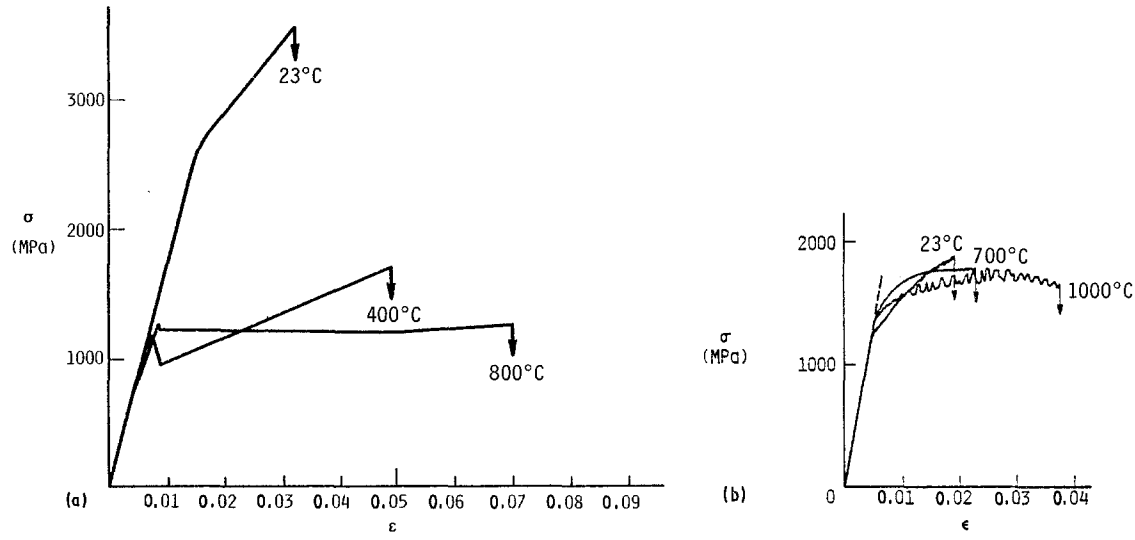

Figure 1 Stress–strain for polycrystalline ZrO_2, $\dot{\varepsilon} = 10^{-5}\,sec^{-1}$. (a) Y-TZP, (b) Mg-PSZ [13].

on to certain specimens, to provide evidence of deformation produced during testing; the latter were characterized by Nomarski microscopy and scanning electron microscopy (SEM), and transmission electron microscopy (TEM) of two-stage carbon surface replicas. Specimens for thin foil TEM were then sectioned, dimpled, and ion milled. Sectioning was performed both normal to the compression axis, and parallel to observed slip planes.

Deformation crystallography for the single crystal material was inferred from single trace Laue X-ray diffraction analysis. Because the only planes previously found to be relevant to slip in zirconia were {0 0 1} and {1 1 1} [7, 8], it was straightforward to decide which, if either, of these possibilities corresonded to the observed surface markings on the polished flats.

3. Results

3.1. Stress–strain behaviour

In Fig. 1, stress (σ) is plotted against axial strain (ε) for polycrystalline Y-TZP tested at a strain rate ($\dot{\varepsilon}$) of $10^{-5}\,sec^{-1}$; included for comparison are recent data [13] for the Mg-PSZ described in Table I. Whereas yield and ultimate strength are very temperature sensitive for Y-TZP, for the magnesia-stabilized material both parameters are temperature insensitive. Regardless of stabilizer chemistry, ductility increases with temperature.

Flow stress curves for the two materials differ in that those for the Y-TZP are smooth and continuous, while the yielding of Mg-PSZ is jerky, or serrated. Furthermore, following initial yield, Y-TZP specimens tested at 400 and 800° C suffered load drops, the amplitude of which decreased with increasing temperature. No such load drops were observed for Mg-PSZ.

The σ-ε behaviour of Y-PSZ single crystals was very sensitive to crystal orientation and temperature. For crystals oriented along ⟨1 2 3⟩ (Fig. 2a), yielding at 23° C took place at a high stress level (nearly 3 GPa), followed by monotonic hardening to an ultimate plastic strain of ~0.005 [6]. At higher temperatures, yield and ultimate strengths were drastically reduced, while strain to failure increased to ~0.06 for $T = 700°$ C. This deformation was realized via a non-hardening, extremely erratic flow process.

Crystals oriented along ⟨1 0 0⟩ behaved in a remarkably different fashion; as shown in Fig. 2b, yielding occurred in two stages. First, at a temperature-dependent stress level during elastic loading, the specimen instantaneously deformed to a plastic strain of 0.0049, at which point elastic deformation resumed. For ambient conditions, the specimen then broke in a brittle mode. At 700° C, on the other hand, specimens yielded via a load drop, followed by smooth, monotonic hardening to an ultimate plastic strain in excess of 0.15.

Yielding was also found to exhibit strain rate sensitivity, an effect most evident at elevated temperatures (Fig. 3). As shown in Fig. 3a, the ⟨1 0 0⟩ single-crystal pre-yield incremental strain plateau again represents a plastic strain of 0.0049, but the stress level at which this occurs is significantly higher with increasing $\dot{\varepsilon}$. Moreover, the macro-yield stress, the amplitude of the load drop, and the ultimate strength all are greater at the higher loading rate, while the

TABLE I Material properties

Material	Flexural strength (MPa)	Hardness (GPa)	Fracture toughness (MPa $m^{1/2}$)	Grain size (μm)/phase	Precipitate size (μm)/phase
Y-PSZ single crystal	1384	13.6	6.9	–/tetragonal (t′)	< 0.01/tetragonal (t) in 0.08 × 0.5/tetragonal (t′)
Y-TZP polycrystal	1000	13.0	8.5	0.5 to 2.0/tetragonal (t)	–
Mg-PSZ polycrystal [9]	600	10.2	8–15	60/cubic	0.05–0.1/tetragonal (t)

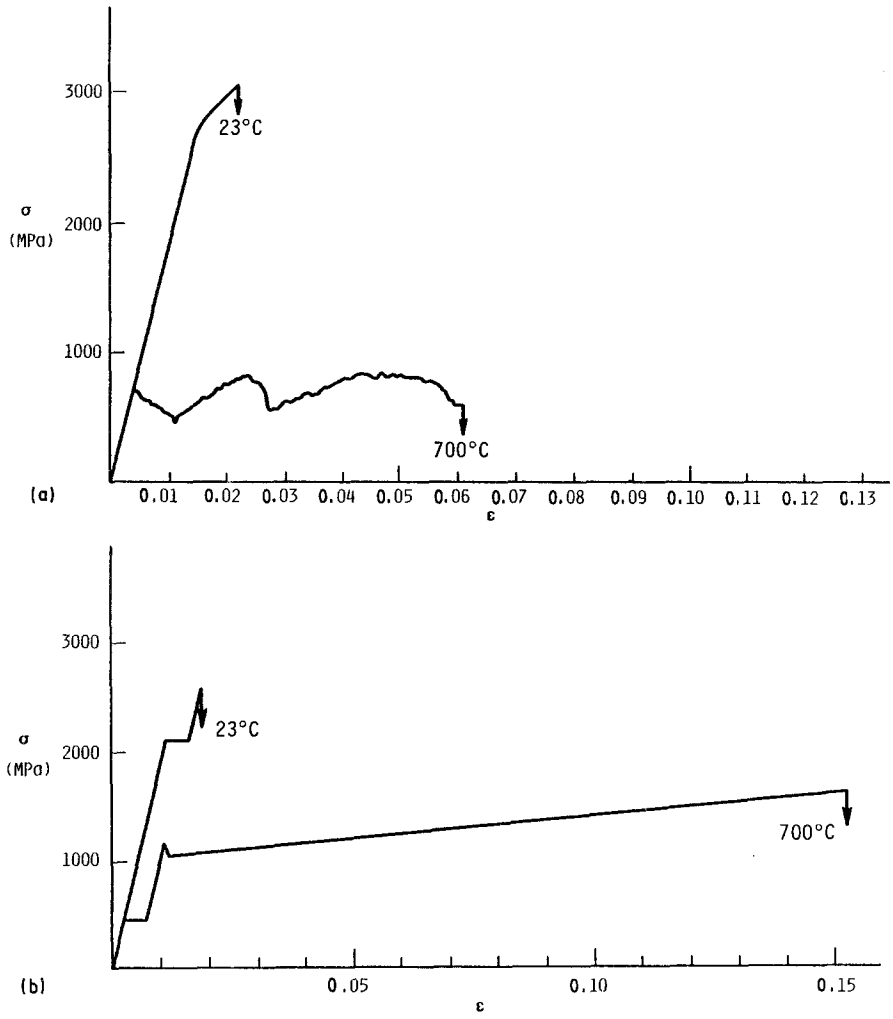

Figure 2 Stress–strain for Y-PSZ single crystals, $\dot{\varepsilon} = 10^{-5}\,\text{sec}^{-1}$. (a) ⟨1 2 3⟩ orientation [13], (b) ⟨1 0 0⟩ orientation.

ductility is significantly reduced. Crystals oriented along ⟨1 2 3⟩ also increased in yield and ultimate strength, and decreased in ductility, with increasing strain rate; however, yielding was never preceded by a load drop.

The strain-rate dependence of Y-TZP deformation (Fig. 3b) was similar to that of the ⟨1 0 0⟩ Y-PSZ single crystals in some respects, but different in one important regard. Again, the material yields prior to the load drop, but this time the rate-dependent yielding takes place over a range of stresses, so that deformation occurs gradually, rather than in a single burst. As for the single crystals, the macroyield point, the amplitude of the load drop, and the ultimate strength increase with strain rate. However, it is surprising to note that as $\dot{\varepsilon}$ increases from 10^{-5} to $10^{-1}\,\text{sec}^{-1}$, there seems to be an increase in ductility. In order to evaluate whether this is indeed a real effect, a few tests were performed at 800° C in a Hopkinson pressure bar (HPB) facility, yielding stress–strain data for $\dot{\varepsilon} = 10^{3}\,\text{sec}^{-1}$. A typical result is shown in Fig. 3b, where it is abundantly evident that by loading at this extremely high rate, both the strength and ductility of the ceramic have been greatly enhanced.

3.2. Deformation and damage mechanisms

In order to obtain some idea of the origin of the ⟨1 0 0⟩ single crystal pre-yield plastic "step", specimens with a polished flat were unloaded immediately following "steps" at both 23 and 700° C. Optical inspection revealed no evidence of deformation, but examination of TEM surface replicas showed (Fig. 4) extensive transformation of plate-like precipitates oriented with their axes (minimum dimension) parallel to the compressive stress axis.

At elevated temperatures ($250 \lesssim T \lesssim 700$° C) the onset of macroscopic yielding for single crystals of both orientations corresponded to the initiation of Luders bands. In the case of the ⟨1 2 3⟩ specimens [13], slip began at one end of the specimen, and propagated throughout the volume by means of planar slip on {0 0 1} ⟨1 1 0⟩ (Fig. 5a). Specimens ultimately failed by shear crack nucleation on {0 0 1} planes. For similarly oriented crystals, this same slip system has been observed for Y-PSZ (8 to 32 wt% Y_2O_3) [11, 12] and for Ca-PSZ [16], tested in compression at $T \cong 1400$° C.

Preceding the ⟨1 2 3⟩ Luders band was a homogeneous transformation of plate-like precipitates visible via TEM of surface replicas. Raman spectroscopy [17] revealed no evidence of monoclinic phase following this transformation. The distribution and size of the precipitates appeared to be essentially the same as that associated with the pre-yield "step" in ⟨1 0 0⟩ specimens.

Specimens of ⟨1 0 0⟩ orientation also yielded via a Luders process, but it was considerably more complex than that observed in the preceding case. The initiation of flow corresponded to the nucleation of intersecting slip bands, which began to propagate down the specimen as deformation proceeded. Shortly afterwards, a second Luders process began, which

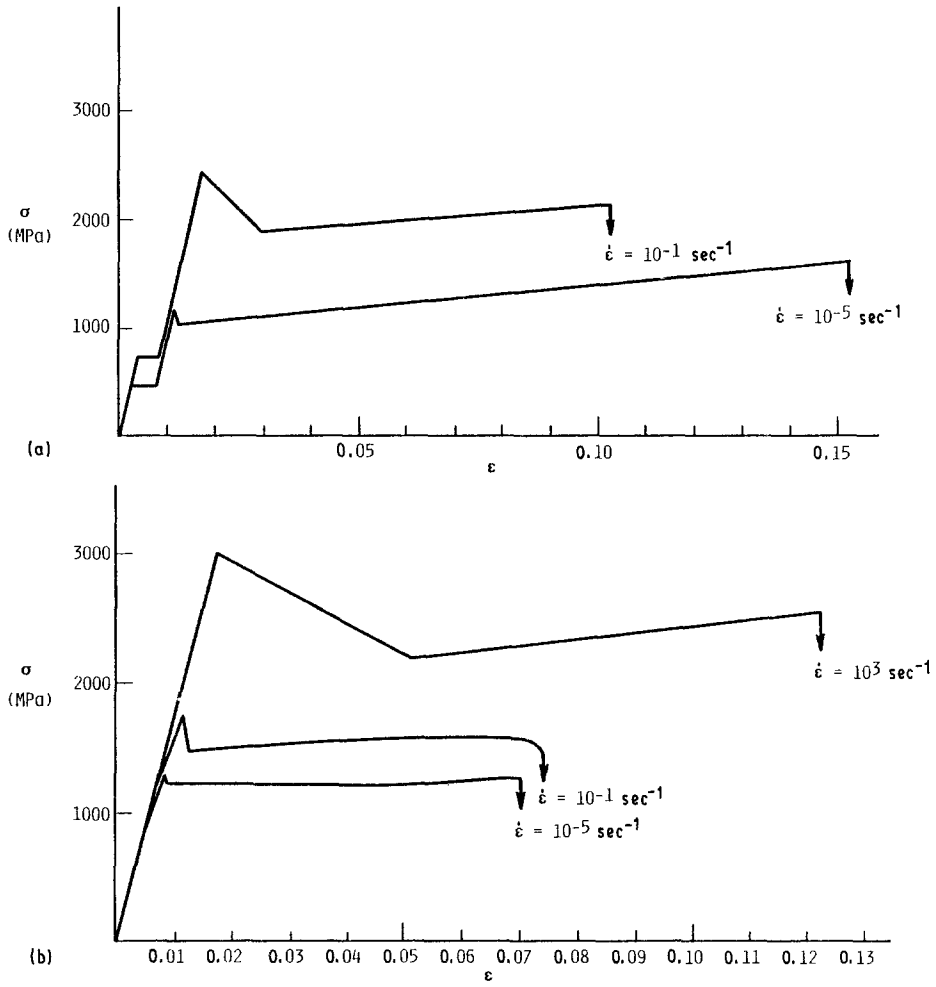

Figure 3 Stress–strain for Y-PSZ and Y-TZP tested at varying strain rate. (a) Y-PSZ, ⟨1 0 0⟩, T = 700° C; (b) Y-TZP polycrystal, T = 800° C.

followed along about a millimeter behind the initial dislocation front. This second front produced marked surface rumpling, and appeared to be caused by massive transformation on intersecting crystallographic planes. An example of a region traversed by both fronts is shown in Fig. 5b; only the transformation plasticity is evident, because the slip markings were destroyed (they could not be resolved using TEM of surface replicas) by the extensive transformation. X-ray diffraction indicated that the trace of the initial slip planes was {1 1 0}, suggesting {1 1 0} ⟨1 $\bar{1}$ 0⟩ slip. (Because the X-rayed flat was a near [0 1 1] orientation, there was no ambiguity in distinguishing between [1 1 0] and {1 1 1}, as there is (only) for the classic [0 0 1] cubic projection.) The trace of the precipitate habit planes, like the slip which preceded it, was duplex on {1 1 0} and {$\bar{1}$ 1 0}.

Transmission electron microscopy of deformed specimens was difficult, due to distortion caused by both transformation-induced strains and by dislocations. At 700° C, the original microstructure of a ⟨1 2 3⟩ crystal is almost unrecognizable (Fig. 6), and many domains are faulted. Extended partial dislocations appear to lie on certain faults (arrows, Fig. 6). Individual dislocations were occasionally observed at combined strains and temperatures as low as 0.005 and 283° C, respectively.

For the multiple slip ⟨1 0 0⟩ orientation, the most frequently observed features are dislocation cells and transformed monoclinic particles. Figs 7a and b show a very high density of dislocations lying within complex {1 1 1} dislocation cell walls. The dislocation density is so high that it is very difficult to image individual dislocations. Many segments seem to be present, evidence of extensive mutual cutting of dislocations on several systems. Other regions exhibit large populations of heavily microtwinned, transformed (t → m) precipitates (Figs 7c and d). Of interest are the numerous microscopic cracks present throughout (arrows), some of which exceed barely 40 nm in length. Microcracks were associated only with transformed monoclinic particles; the cracks

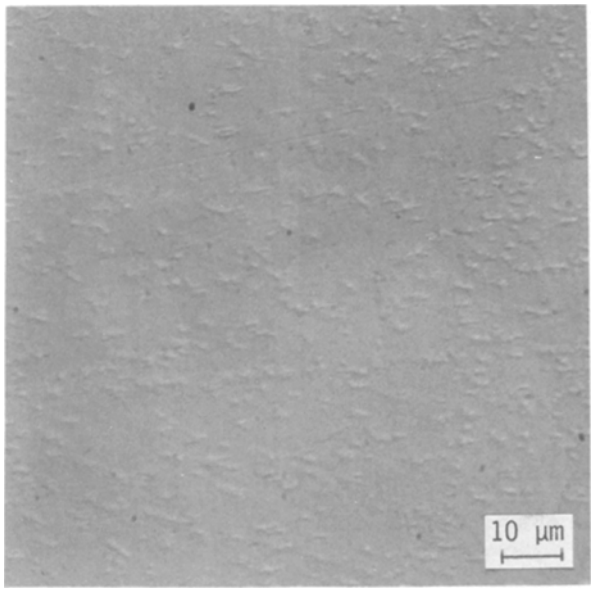

Figure 4 Precipitate transformation during ⟨1 0 0⟩ single crystal preyield plastic "step" at T = 23° C. Stress axis is roughly vertical.

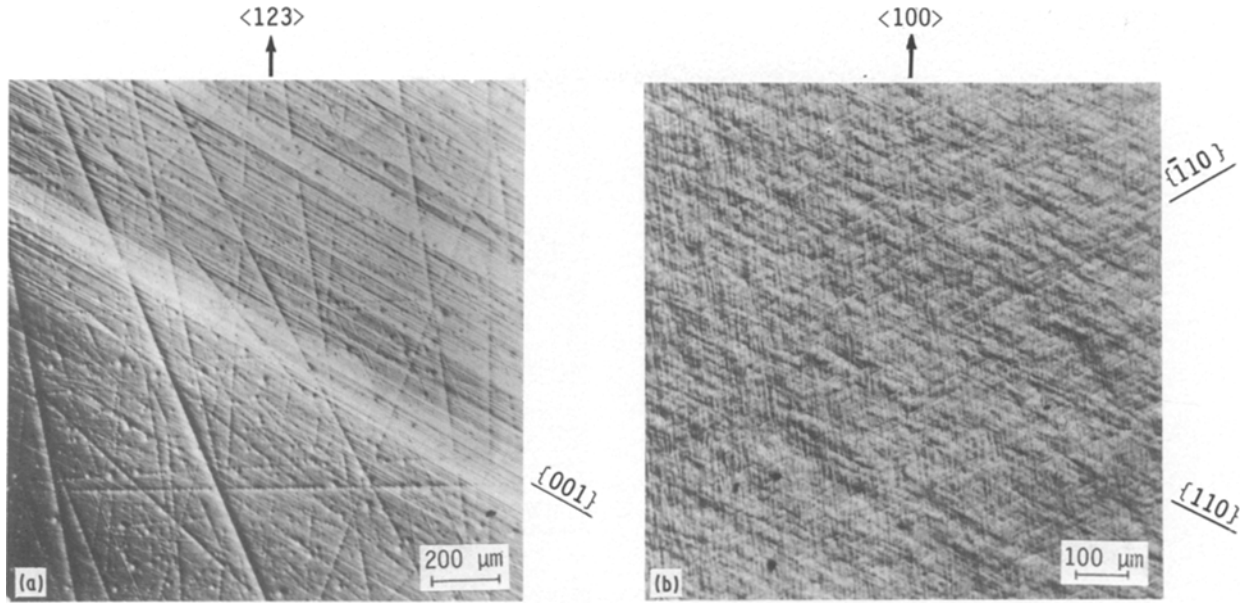

Figure 5 Nomarski contrast evidence of single crystal Y-PSZ deformation at $T = 700°C$, $\dot{\varepsilon} = 10^{-5}\,sec^{-1}$. (a) ⟨1 2 3⟩ orientation, $\varepsilon = 0.015$, showing planar slip bands [13]. (b) ⟨1 0 0⟩ orientation, $\varepsilon = 0.03$, showing surface rumpling caused by precipitate transformation.

usually spanned the minimum precipitate dimension, and were never observed within dislocation tangles or cells.

At room temperature, the ⟨1 0 0⟩ crystals failed in a brittle mode, while the ⟨1 2 3⟩ specimens deformed slightly (Fig. 2) prior to failure. However, the latter displayed no slip line evidence of dislocation activity; instead, TEM replica study again revealed evidence of plate-like precipitates similar to those observed following the pre-yield incremental strain steps in the ⟨1 0 0⟩ crystals.

These single crystal deformation mechanisms seem to invite comparison with those characteristic of Y-TZP. For example, the gradual deformation of polycrystalline specimens which preceded their macro-yield load drop at all temperatures was accompanied by extensive, homogeneous transformation (Fig. 8). However, the likelihood of fundamental differences between this yield behaviour, and the single crystal pre-yield incremental strain step, will be shown.

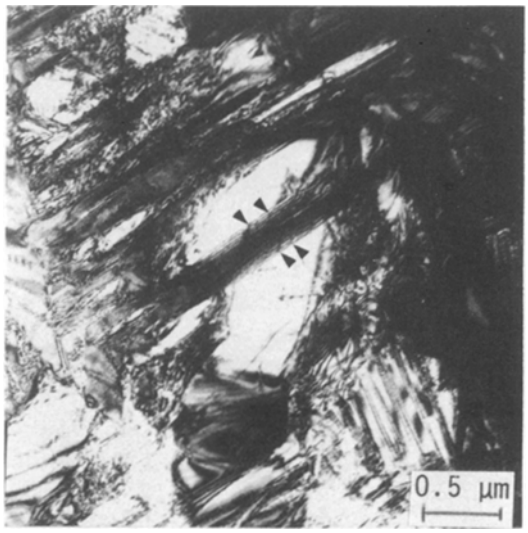

Figure 6 TEM of ⟨1 2 3⟩ crystal [13], $T = 700°C$, $\varepsilon = 0.015$. Foil is normal to ⟨1 2 3⟩.

The bulk yielding process in Y-TZP was clearly different, and is shown in Fig. 9 for a specimen tested at 800° C. Again specimens yielded through the nucleation and propagation of a Luders front, but here (Fig. 9a) it is one whose passage yields imhomogeneous, intersecting shear bands. Closer inspection shows that the bands have rather a dimpled appearance (Fig. 9b), evince no dislocation slip, and are separated by blocks of apparently undeformed material. The bands are oriented at an average angle of 45° relative to the compressive stress axis.

Transmission replica microscopy (Fig. 10a) shows that the deformation bands are actually regions in which high shear strains are accommodated by grain-boundary sliding, with attendant formation of intergranular, axial microcracks. Upon inspection of the figure, it can be seen that within the shear bands, grain boundaries are generally visible, whereas they are invisible within the relatively undeformed blocks adjacent. The basis for this effect can be seen in Figs 10b and c, where it is evident that the grain boundaries are decorated by small, roughly spherical, cavities which have nucleated on certain facets, and, frequently coalesced to form grain-sized microcracks. The latter can then coalesce to form larger, multigrain size cracks, especially where shear bands intersect (Fig. 11). Such sites become the origins of localized failure (Fig. 12a), i.e. regions of gross intergranular separation (Fig. 12c) created by high local shear strains (Fig. 12b).

The situation just described is complicated by other factors. Prior to deformation, grain boundaries are smooth, and grain interiors are relatively free of defects (Fig. 13a). During initial yielding, transformation of tetragonal phase occurs (Fig. 13b), as manifested in the surface relief described earlier (Fig. 8). However, as deformation proceeds, originally smooth grain boundaries begin to assume a wavy profile (arrows, Fig. 13c). The "waves" often seem to be associated with local transformed regions. At other

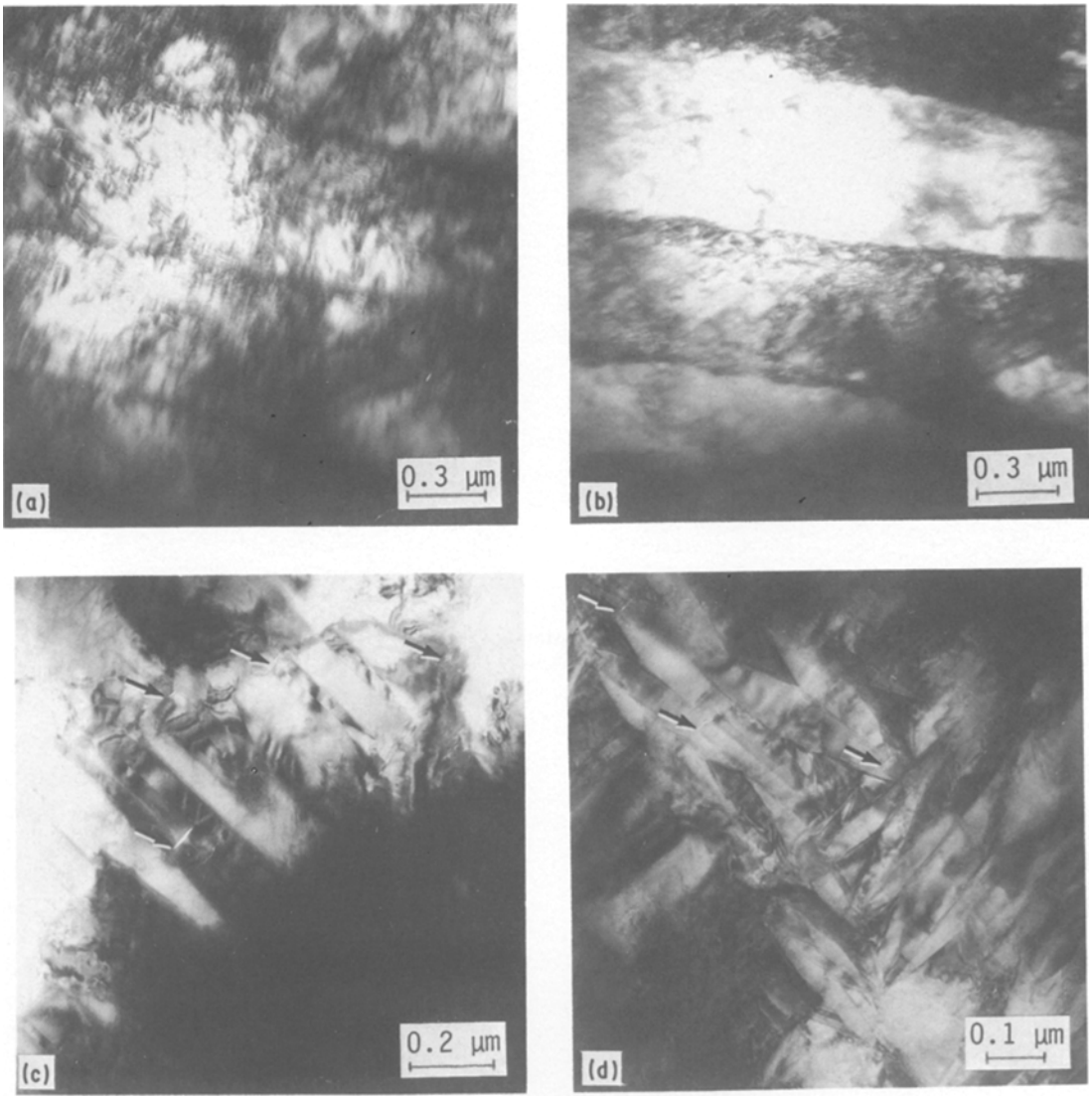

Figure 7 TEM of ⟨1 0 0⟩ crystal, $T = 700°C$, $\dot{\varepsilon} = 0.03$. Foil is normal to ⟨1 0 0⟩. (a) Dislocation tangles and {1 1 1} cell walls. (b) Tilted view of (a). (c) Transformed particles, and associated microcracks (arrows). (d) Transformed particles, and associated microcracks (arrows).

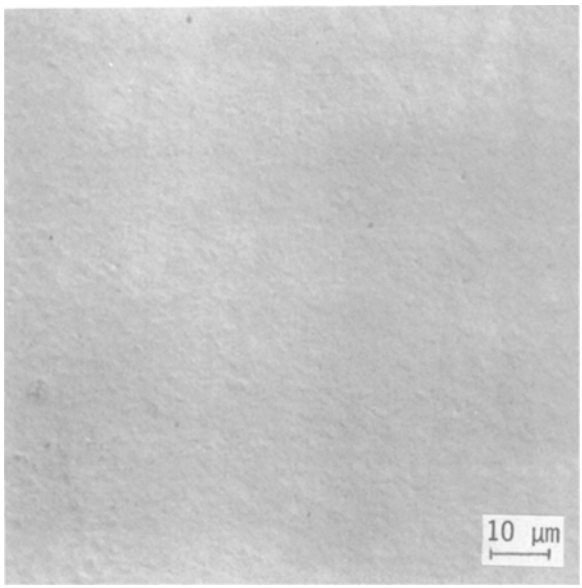

Figure 8 Nomarski contrast view of surface rumpling caused by transformation of polycrystalline Y-TZP deformed within preyield region, $T = 23°C$, $\dot{\varepsilon} = 10^{-5}\ sec^{-1}$. Stress axis is vertical.

locations, cusps develop at the intersections of transformed layers and grain boundaries (arrow, Fig. 13d).

The development of damage in Y-TZP, as outlined above, is markedly different from that which accompanies inelastic deformation (Fig. 1b) in Mg-PSZ. The latter has been discussed elsewhere [8], and treated theoretically by Chen and Reyes-Morel [3], but will be briefly outlined here for the sake of contrast. At all temperatures, plastic flow is realized by shear localization initiated by autocorrelated precipitate transformation (t – m) [9]. These multiple microscopic events produce families of macroscopic shear bands lying within deformed grains. As the temperature rises, the bands increase in width, so that the local shear displacement for a given shear strain is larger. Furthermore, axial cracking shifts from transgranular to intergranular with increasing temperature. On the other hand, little strain seems to be associated with GB sliding, at least for $T \gtrsim 1000°C$, and there are no "superplastic" GB shear instabilities, such as those which were observed for Y-TZP, and which account for most of the plastic strain in the latter.

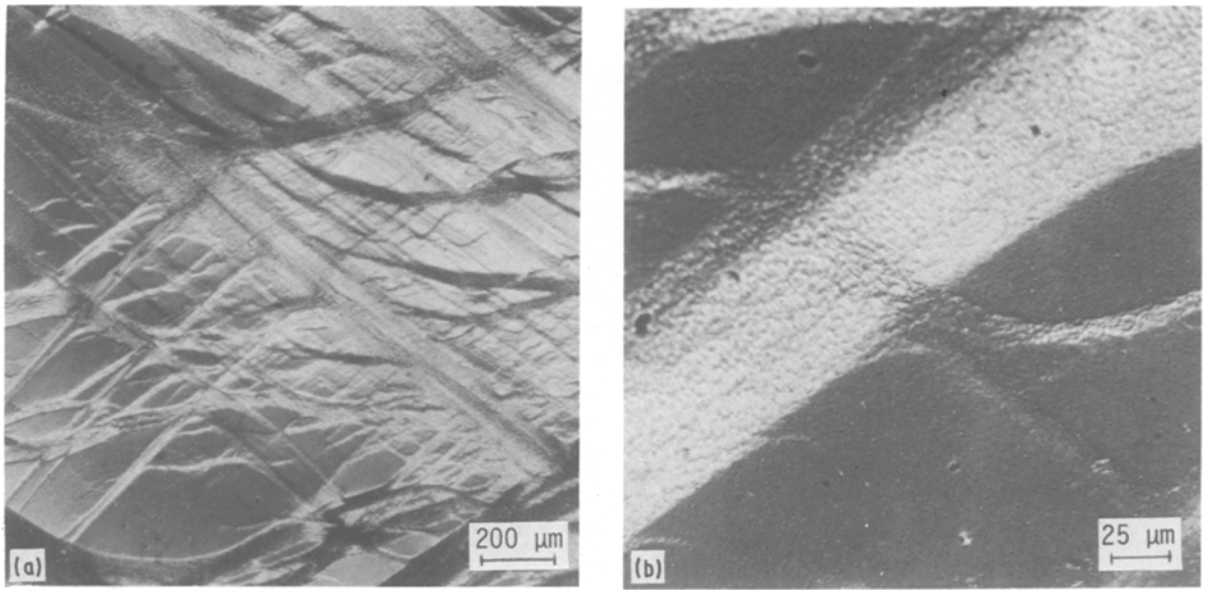

Figure 9 Nomarki contrast view of Y-TZP to $\varepsilon = 0.05$ at $T = 800°C$, $\dot{\varepsilon} = 10^{-5}\,sec^{-1}$. Stress axis was vertical. (a) Deformation in wake of Luders front, showing inhomogeneous shear bands. (b) Higher magnification of typical deformation band, showing fine scale rumpling, and no slip lines.

4. Discussion

4.1. Single-crystal deformation

Recalling the behaviour of the single crystal Y-PSZ, it is clear that at least some similar behaviour is involved in the deformation of specimens of both orientations at equivalent strain rates and temperatures. For example, a precipitate transformation is responsible, at all temperatures, for the pre-yield incremental strain step for $\langle 1\,0\,0\rangle$ crystals, and a similar process seems to accompany yielding at 23° C for $\langle 1\,2\,3\rangle$ specimens. In addition, extensive post-yield plastic flow at intermediate temperatures is realized via dislocation Luder's bands, supplemented by varying contributions from t → m transformations. These observations, as well as certain seemingly dissimilar aspects, can be rationalized as follows.

Because essentially no monoclinic phase is present immediately following the pre-yield "step", it seems most likely that the observed plasticity is caused by ferroelastic domain reorientation, along the lines proposed by Virkar and Matsumoto [6]. Furthermore, as all of one set of tetragonal precipitate c-axes are directly in line with the compressive stress axis, it is entirely reasonable that for $\langle 1\,0\,0\rangle$ crystals, the transformation is complete, and the "step" takes place, at a single stress amplitude (for a given temperature and strain rate).

For $\langle 1\,2\,3\rangle$ crystals, on the other hand, the compressive axis lies at an angle to all of the $\{1\,0\,0\}$ planes, so that ferroelasticity should occur over a range in stress. The onset of transformation presumably would correlate with the normal stress on the most favoured set of planes, i.e. (1 0 0), being roughly equal to that required to produce the pre-yield step in $\langle 1\,0\,0\rangle$ crystals. The latter stress at $T = 23°C$ and $\dot{\varepsilon} = 1 \times 10^{-5}\,sec^{-1}$ was 2100 MPa; taking into account the stress axis/(1 0 0) planar angle, it would be predicted that ferroelastic reorientation of $\langle 1\,0\,0\rangle$ c-axis precipitates should initiate at an axial stress level of ~ 3000 MPa. This is reasonably close to the observed $\langle 1\,2\,3\rangle$ "yield" stress of ~ 2600 MPa. This agreement, and especially the association of $\langle 1\,0\,0\rangle$ transformations with c-axis compression, constitutes a strong argument for ferroelasticity, as opposed to an earlier suggestion [13] involving cubic to rhombohedral transformation, as the basis for the observed transformation-induced strains.

Based on the $\langle 1\,0\,0\rangle$ crystal results, it is obvious that the proposed ferroelastic effect is affected by strain rate and temperature. There appear to be two possible rationales for this behaviour, the first being that ferroelastic domain switching is an intrinsically thermally activated process, involving migration of the interfaces separating the domains. As stress is applied along [0 0 1], the variants with their c-axes parallel to [1 0 0] and [0 1 0] are encouraged to grow at the expense of [0 0 1] variants. The $\{1\,0\,1\}$ interfaces separating these domains move to consume the [0 0 1] variants. This migration process involves a shear distortion of the zirconia sublattice accompanied by a oxygen-ion hopping from one position to another, from [1/4, 1/4, 1/4 + ∂] to [1/4 + ∂, 1/4, 1/4]. At low temperature, the potential energy barrier between these two sites is probably higher than at high temperature; thus, a larger stress is required at low temperature to produce the same probability of a thermally activated jump as occurs at higher temperatures. In addition, the interface migration process involves a certain amount of friction due to the small shifts in the oxygen ions.

Another possibility is that associated with the ferroelastic precipitate shape change is a thermally activated matrix accommodation, which also could affect subsequent macroplastic flow. In particular, dislocations are probably punched out by each colony undergoing a ferroelastic reorientation. During switching, the shape of the colony is elongated normal to the stress axis. The nucleation of misfit dislocations

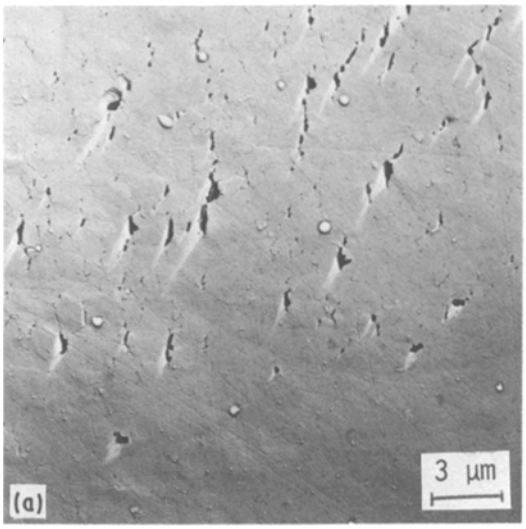

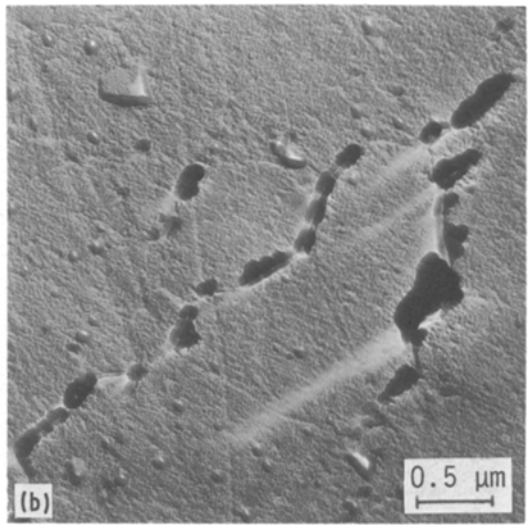

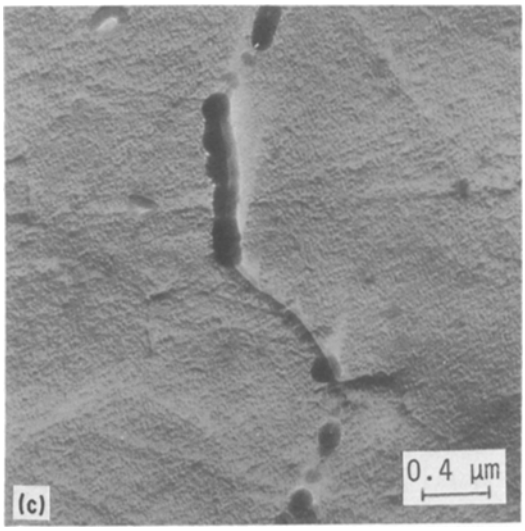

Figure 10 TEM replica of deformation shear bands in Y-TZP, $\varepsilon = 0.05$, $T = 800°C$, $\dot{\varepsilon} = 10^{-5}\,sec^{-1}$. Stress axis is vertical. (a) Deformation band with axial intergranular cracks and visible grain boundaries. (b) Multiple-cavitated grain-boundary microcrack via cavity coalescence.

required to accommodate this strain is also expected to be thermally activated. This dislocation punching represents a distinct difference between ferroelastic domain reorientation and the classic t–m martensitic reaction; in the martensitic reaction, the lowered symmetry of the product phase allows the shear strains associated with the transformation to be accommodated by internal microtwinning. Conversely, twins are eliminated by the process of ferroelastic reorientation, and the shape change must be accommodated by another mechanism.

If thermally activated dislocation flow is associated with the ferroelastic effect in t-precipitates, it will then control the stress level at which such transformations take place for a given temperature and strain rate, while the essentially constant volume (number per specimen) of transforming (switching) precipitates should yield a roughly constant incremental strain. This is precisely the behaviour observed for $\langle 1\,0\,0\rangle$ crystals. Dislocation accommodation can be envisaged to arise as follows.

It is evident that compressive loading of the $\langle 1\,2\,3\rangle$ crystal provides not only a compressive stress component along the c-axis of one t′ variant, but also a significant shear component along [1 1 0] (0 0 1). While the compressive stress provides a driving force for reorientation, the shear component is available to drive dislocations on the observed slip system. Ferroelastic reorientation of some t′ colonies and not others, results in concentrated shear stresses at the interface between colonies which will require nucleation of misfit dislocation loops of [1 0 0] Burgers vector (Fig. 14). These loops would dissociate into [1 1 0] and [1 $\bar{1}$ 0] segments, and the applied stress would tend to drive the [1 1 0] (0 0 1) segments through the crystal.

Such a process might also account for the behaviour of $\langle 1\,2\,3\rangle$ crystals at 700° C. Taking into account the angle between the stress axis and the (1 0 0) plane, it would be estimated on the basis of the $\langle 1\,0\,0\rangle$ crystal results that ferroelastic switching (yielding) in $\langle 1\,2\,3\rangle$ specimens would commence at ~ 700 MPa, as observed. However, the stress would then be relaxed (again as observed) by the avalanching of misfit

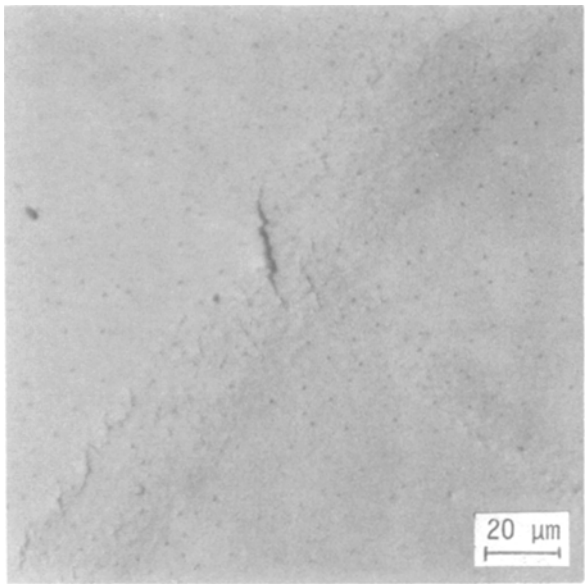

Figure 11 Microcrack formation at intersection of shear bands in Y-TZP. Stress axis is vertical, $\varepsilon = 0.05$, $T = 800°C$, $\dot{\varepsilon} = 10^{-5}\,sec^{-1}$.

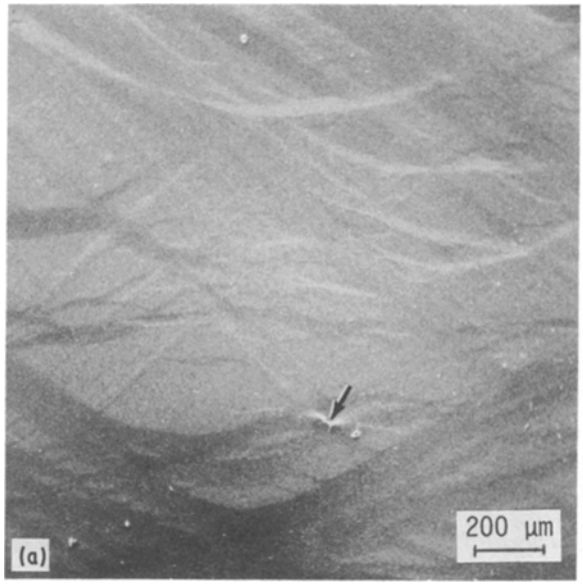

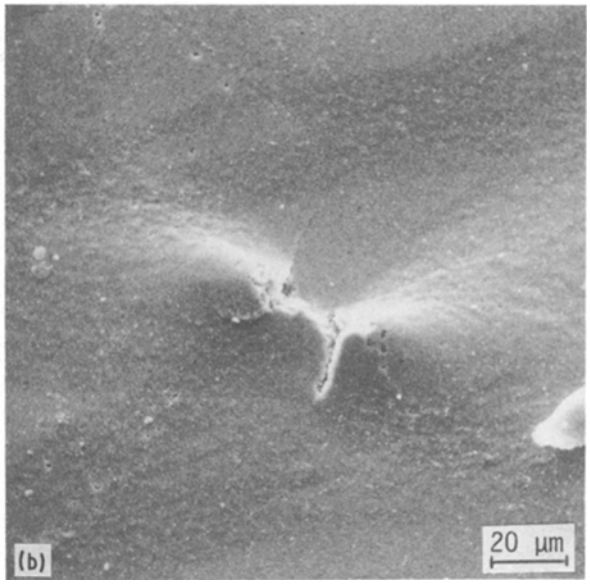

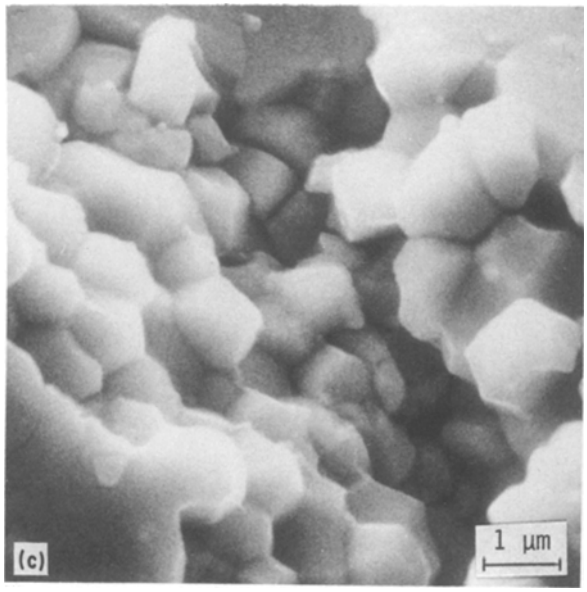

Figure 12 Localized intergranular failure at site of shear band intersection in Y-TZP. $\varepsilon = 0.05$, $T = 800°\,C$, $\dot{\varepsilon} = 10^{-5}\,sec^{-1}$. Stress axis is vertical. (a) Localized damage (arrow) at intersection of shear bands. (b) Higher magnification view of (a), showing intense local shear deformation. (c) Higher magnification view of (b), showing intergranular separation.

dislocations through the crystal, creating an autocatalytic Luders process. This process is inherently unstable, and would account for the jerky nature of the flow curve. The specimen finally fails in shear when the single slip system is exhausted, and slip band cracks nucleate.

In the case of $\langle 1\,0\,0\rangle$ crystals, on the other hand, the resolved shear stress on the misfit dislocation $(0\,0\,1)$ slip planes is essentially zero, hence, as expected, no deformation takes place immediately following the pre-yield "step". Instead slip is eventually activated on the next most favoured system, $\{1\,1\,0\}\ \langle 1\,\bar{1}\,0\rangle$. It should be noted that Dominguez-Rodriguez *et al.* [11], observed $\{1\,1\,1\}\ \langle 1\,\bar{1}\,0\rangle$ slip in near (4°) $\langle 1\,0\,0\rangle$ 16.9 wt % Y-PSZ crystals tested at 1400° C. However, the temperature was much higher than in the present case (1400° C compared to 700° C). Furthermore, the microstructure was very different, due to the yttria content (16.9 wt % compared to 5%). Finally, the Schmid factor for $\{1\,1\,1\}\ \langle 1\,\bar{1}\,0\rangle$ slip was 0.47 in the work of Dominguez-Rodriguez *et al.*, compared with the present 0.408; in both cases, the Schmid factor for $\{1\,1\,0\}\ \langle 1\,\bar{1}\,0\rangle$ slip was 0.5. Based on the experimental differences, and the greater disparity in resolved shear stress on the competing slip systems, the results obtained seem reasonable.

Because multiple planes are involved, due to the loading symmetry, flow of $\langle 1\,0\,0\rangle$ crystals is stable and hardening. It is this stable dislocation flow which accounts for the remarkably high ductility of $\langle 1\,0\,0\rangle$ compared to $\langle 1\,2\,3\rangle$ crystals. Furthermore, because a transformation Luders front follows the initial multislip front through the crystal, while a corresponding one does not follow the $\langle 1\,2\,3\rangle$ crystal single slip dislocations Luders front, it is likely that the transformations were nucleated by local stresses at dislocation pile-ups, etc. The specimen apparently failed by the coalescence of the transformation-nucleated microcracks; thus, its demise was ultimately related to the deformation which, for a period, had extended its life.

4.2. Polycrystalline deformation

It will be recalled that Y-TZP specimens yielded gradually, before either failing (at 23° C) or experiencing a load drop followed by macroscopic strain ($T \gtrsim 400°\,C$). The yield stress level was thermally activated (it decreased with temperature and rose with strain rate), and was associated with surface rumpling due to transformations. This is qualitatively similar to the single crystal observations discussed above, in which the strain was attributed to ferroelastic domain switching.

However, Raman spectroscopy [17] permitted the elimination of the t → m transformation as a basis for the single-crystal effect; such evidence was unfortunately unavailable for the present Y-TZP. Furthermore, recent experiments by Virkar and Matsumoto [18] have shown that, based on X-ray evidence, both grinding and uniaxial compression produced ferro-

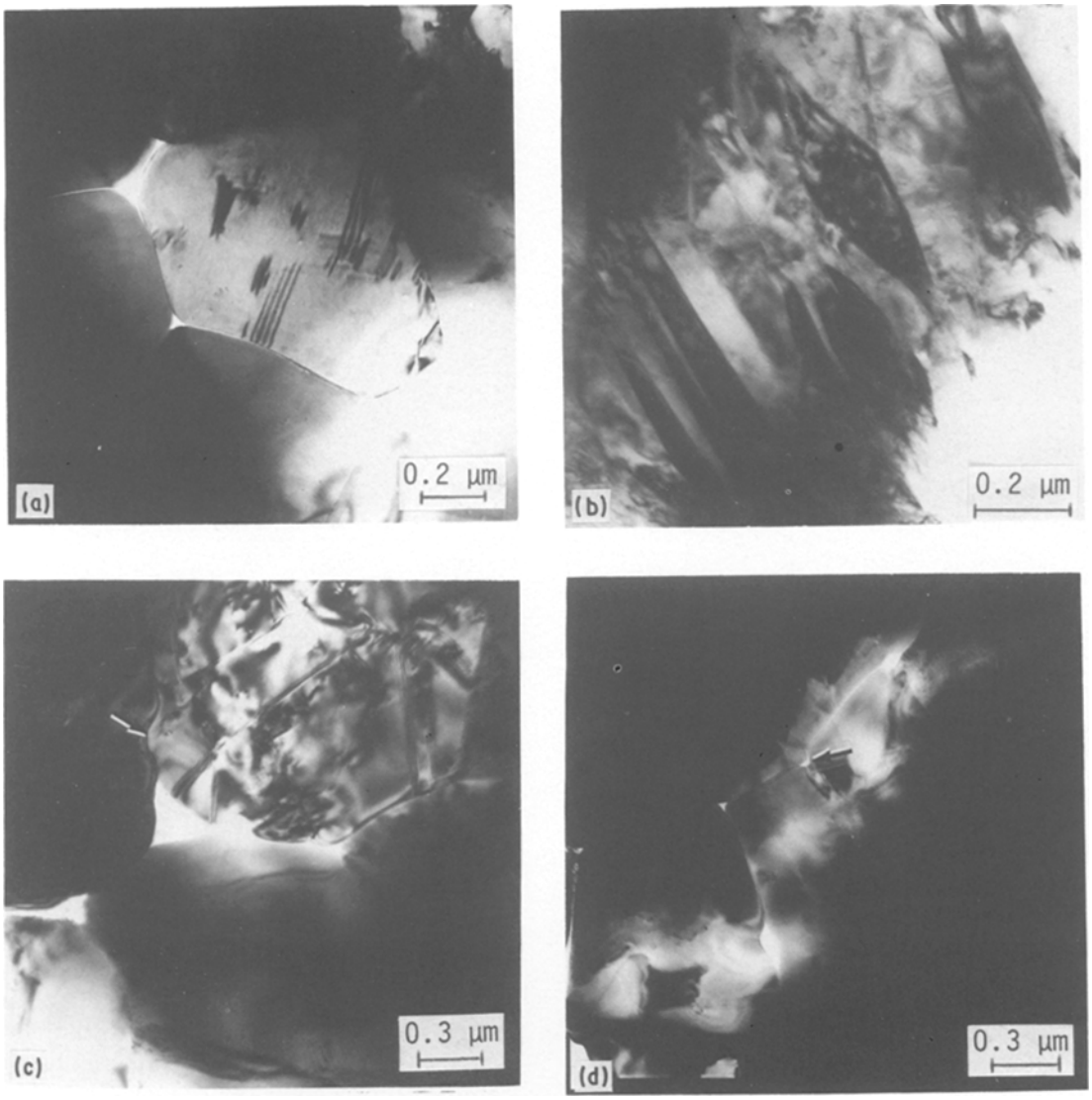

Figure 13 Transmission electron microscopy of Y-TZP specimen deformed to a strain of 0.05 at $T = 800°C$, $\dot{\varepsilon} = 10^{-5}\ sec^{-1}$, compared with undeformed microstructure. (a) Undeformed microstructure. (b) Deformation-induced tetragonal to monoclinic transformation. (c) Deformation-induced grain-boundary waviness (arrow). (d) Transformation-induced grain-boundary cusps (arrow).

elastic domain switching in Ce-TZP, but not in Y-TZP. Instead, increased monoclinic phase was observed in the yttria-stabilized material. The latter experiments suggest the likelihood of the t → m transformation as the basis for the observed plasticity.

Fortunately, this conclusion seems to be compatible with the thermally activated nature of the transformation of tetragonal grains to the monoclinic phase. For example, Ruhle *et al.* [7] have recently observed the dynamics of the t → m transformation of Y-TZP, and found that it can be remarkably sluggish. Yttria content varies from grain to grain, and can deviate significantly from the average; regions of reduced Y_2O_3 content correspond to increased likelihood of nucleation, hence increased speed of transformation. In addition, Andersson *et al.* [19], have observed that some Y-TZP variants (of roughly the same grain size and Y_2O_3 concentrations as the present material) do not twin internally when they transform to monoclinic. Rather, the change in shape is thought to be accommodated by matrix strain and GB dislocation generation; the latter process would be thermally activated.

Finally, such a scenario is compatible with the continuous, non-step nature of the transformation strain. Activation of grains of different size, shape, orientation relative to the stress axis, and stabilizer content would correspond to a range of stress levels, and the observed strain "hardening".

The macroscopic yielding of the polycrystalline ZrO_2 is not at all comparable with the dislocation mechanisms responsible for flow in single crystals. This is not surprising, considering the inverse strain rate effect shown in Fig. 3. The behaviour of the $\langle 1\,0\,0 \rangle$ single crystal (Fig. 3a) represents a classic example of the suppression of dislocation motion (decreased ductility), and a corresponding increase in strength, with increasing strain rate. The polycrystalline material, on the other hand, is not only strengthened, but its ductility is enhanced as well, with more rapid loading (Fig. 3b). This curious and possibly unique effect is probably due either to delay in the onset of instability represented by nucleation and growth of the shear bands themselves, or to retardation of the creep cavitation process responsible for shear band failure. It is interesting that the energy of failure

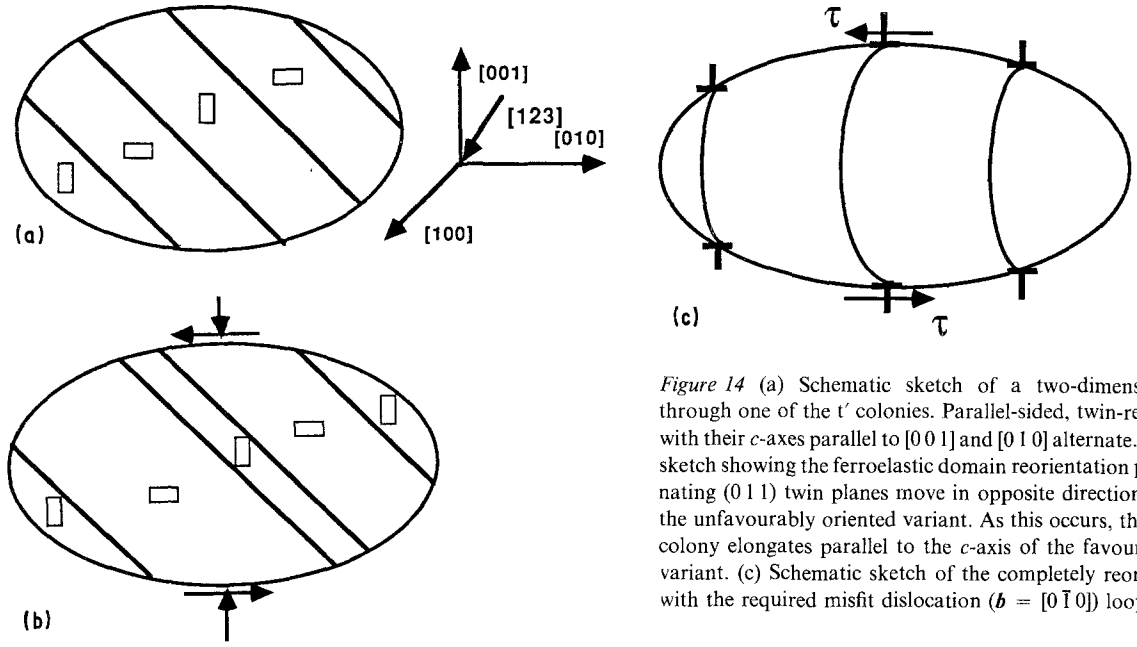

Figure 14 (a) Schematic sketch of a two-dimensional section through one of the t′ colonies. Parallel-sided, twin-related variants with their *c*-axes parallel to [0 0 1] and [0 1 0] alternate. (b) Schematic sketch showing the ferroelastic domain reorientation process. Alternating (0 1 1) twin planes move in opposite directions to consume the unfavourably oriented variant. As this occurs, the shape of the colony elongates parallel to the *c*-axis of the favourably oriented variant. (c) Schematic sketch of the completely reoriented colony with the required misfit dislocation ($\boldsymbol{b} = [0\,\bar{1}\,0]$) loops.

at $\dot{\varepsilon} = 10^3\ \text{sec}^{-1}$, calculated on the basis of the area under the stress–strain curve, is nearly four times that obtained for $\dot{\varepsilon} = 10^{-5}\ \text{sec}^{-1}$.

The formation and evolution of the compressive shear bands affords an interesting comparison with the recent work by Dalgleish and co-workers [20, 21], on creep rupture during bending of polycrystalline alumina. For the latter relatively fine-grained (4 μm) material, characterized by a glassy grain-boundary phase, failure in the absence of large pre-existing flaws was caused by the coalescence of facet-sized, shear band microcracks. The microcracks nucleated via cavitation and cavity link-up on planes normal to the tensile axis, and congregated into shear bands whose normal projections were, on average, about 60° from the stress axis. Many bands were observed [20] to initiate at microstructural or chemical heterogeneities. Testing was performed at constant stress at temperatures $\geqslant$ 1250° C, with shear band formation occurring only for specimens which failed via creep damage coalescence at strains in excess of 0.08. At smaller strains, failure occurred by the growth of a single dominant crack nucleated at an inherent processing flaw. Shear banding was not observed on the compressive sides of the failed bend specimens.

Testing of the present ZrO_2 material was performed at constant strain rate, although once the material began to flow at 800° C, the stress remained essentially constant (Fig. 1a). Deformation development differed markedly from that observed for the Al_2O_3 tested in bending [20, 21], in that shear bands (which again corresponded to large failure strains, i.e. $\varepsilon_f \simeq 0.07$) were observed in compression. It is likely that the alumina [14, 15] simply failed in tension before the compressive stress reached the level required for the nucleation of shear bands.

As for the Al_2O_3, cavitation and microcrack nucleation (cavity coalescence) in the zirconia took place on grain boundaries approximately normal to local tensile stresses, i.e. on facets containing the compression axis. However, the shear bands within which these processes occurred did not lie at 30° to the principal stress axis, as they did for tensile loading of alumina [20, 21]. Instead, the bands were oriented roughly 45° to the stress axis, and they never seemed to be associated with material flaws. This suggests that the damage localization manifested in the bands probably derived from an instability within a homogeneous deformation process.

This sort of situation has been analysed theoretically by Rudnicki and Rice [22] for the case of multiple microfracture of brittle materials, leading to shear faulting. The present case is different, to the extent that the "pre-existing flaws" are not randomly oriented fissures, but rather are inclined grain boundaries which at elevated temperature may slide to permit cavitation on adjacent boundaries containing the compressive load axis. The sliding boundaries are "lubricated" by the viscous GB phase, a factor not included in the treatment of Rudnicki and Rice [22]. Nevertheless, the latter indicates that for reasonably low coefficients of sliding friction, the inclination of shear bands relative to the stress axis is dominated by dilatation. Extensive cavitation and associated multigrain macrocracks produce high dilatation, as obtained in the tensile experiments of Dalgleish *et al.* [20, 21]. The pertinent deformation localization analysis [22] predicts an angle of shear band inclination of $\sim 60°$, as observed experimentally [21].

In the present zirconia compression experiments, it is evident that shear band dilatation is low. The predominant damage features seem to be isolated cavities, and widely dispersed, facet-sized microcracks. Under such circumstances, the theoretically predicted [22] shear-band angle of incidence would be $\sim 45°$. This prediction is borne out experimentally (Fig. 9a).

5. Concluding remarks

It is evident that for both single-crystal and polycrystalline Y-PSZ, failure is governed by the development of shear instabilities. The latter are an inevitable consequence of the deformation mechanisms (martensitic and/or thermally activated transformations, dislocation activity, grain-boundary sliding/cavitation)

which impart higher toughness to this class of ceramic alloy. It is interesting to observe that the materials resemble metals, to the extent that they do in fact deform, and that their uniaxial compressive-to-tensile strength ratio is much lower than that usually found for ceramics, i.e. $8 \lesssim \sigma_C/\sigma_T \lesssim 20$. For metals, $\sigma_C/\sigma_T \simeq 1$, which is essentially the case for single-crystal and polycrystal Y-PSZ at $T \lesssim 700°$ C; even at $T = 23°$ C, the Y-PSZ compressive–tensile strength ratio is $\lesssim 3$. These low ratios can be rationalized by applying yield criteria based on shear and dilatation, as outlined recently by Chen and Morel [3].

The shear-band deformation of the polycrystalline Y-PSZ takes place at a surprisingly low temperature. This suggests that with modest adjustments in loading rate, grain size, and/or confinement (to control dilatation) it might be possible to suppress shear band formation and cavitation, and achieve, in the temperature range 700 to 800° C, the homogeneous GB sliding required for superplastic forming. Recent work by Wakai *et al.* [23], has shown that superplastic flow of 0.3 μm Y-PSZ is possible at strain rates on the order of 10^{-4} sec^{-1}, but requires a temperature of at least 1450° C. It will be recalled that the present Y-PSZ tetragonal grains were on the order of 0.5 μm in size, and test temperatures did not exceed 800° C.

Conversely, creep resistance obviously could be improved by a large grain size, and the use of a sintering aid characterized by higher viscosity at intermediate temperatures. It would be expected that the resulting polycrystalline material would then be forced to deform by the dislocation and transformation mechanisms observed in the single-crystal work.

Acknowledgements

The support of the Office of Naval Research under Contract No. N00014-84-C-0213 is gratefully acknowledged. Thanks are expressed to T. W. Coyle for provision of the single crystals, and to the Norton Company for provision of the polycrystalline zirconia.

References

1. A. G. EVANS and R. M. CANNON, *Acta Metall.* **34** (1986) 761.
2. E. P. BUTLER, *Mater. Sci. Technol.* **1** (1985) 417.
3. I-W. CHEN and P. E. REYES-MOREL, *J. Amer. Ceram. Soc.* **69** (1986) 181.
4. M. V. SWAIN, *Acta Metall.* **33** (1985) 2083.
5. R. CHAIM, M. RUHLE and A. H. HEUER, *J. Amer. Ceram. Soc.* **68** (1985) 427.
6. A. V VIRKAR and R. L. K. MATSUMOTO, *ibid.* **69** (1986) C-224.
7. M. RUHLE, N. CLAUSSEN and A. H. HEUER, in "Advances in Ceramics, Vol. 12, Science and Technology of Zirconia II", edited by N. Claussen, M. Ruhle and A. H. Heuer (American Ceramic Society, Columbus, Ohio, 1984) p. 352.
8. G. WAHLBERG, L. K. L. FALK, G. L. DUNLOP and K.-O. AXELSSON, *J. Mater. Sci. Lett.* **4** (1985) 1353.
9. J. LANKFORD, *J. Mater. Sci.* **20** (1985) 53.
10. V. LANTERI, A. H. HEUER and T. E. MITCHELL, in "Advances in Ceramics, Vol. 12, Science and Technology of Zirconia II", edited by N. Claussen, M. Ruhle and A. H. Heuer (American Ceramic Society, Columbus, Ohio, 1984) p. 118.
11. A. DOMINGUEZ-RODRIGUEZ, K. P. D. LAGERLOF and A. H. HEUER, *J. Amer. Ceram. Soc.* **69** (1986) 281.
12. A. DOMINGUEZ-RODRIGUEZ, V. LANTERI and A. H. HEUER, *ibid.* **69** (1986) 285.
13. J. LANKFORD, *J. Mater. Sci.* **21** (1986) 1981.
14. R. P. INGEL, PhD thesis, The Catholic University of America (1982).
15. L. J. SCHIOLER, R. N. KATZ, A. C. GONZALEZ and B. R. LAWN, *Ceram. Bull.* **64** (1985) 326.
16. M. L. MECARTNEY, W. T. DONLON and A. H. HEUER, *J. Mater. Sci.* **15** (1980) 1063.
17. T. COYLE, personal communication (1985).
18. A. V. VIRKAR and R. L. K. MATSUMOTO, unpublished research (1986).
19. C. A. ANDERSSON, J. GREGGI and T. K. GUPTA, in "Advances in Ceramics, Vol. 12, Science and Technology of Zirconia II", edited by N. Claussen, M. Ruhle and A. H. Heuer (American Ceramic Society, Columbus, Ohio, 1984) p. 78.
20. B. J. DALGLEISH, E. B. SLAMOVICH and A. G. EVANS, *J. Amer. Ceram. Soc.* **68** (1985) 575.
21. B. J. DALGLEISH and A. G. EVANS, *ibid.* **68** (1985) 44.
22. J. W. RUDNICKI and J. R. RICE, *J. Mech. Phys. Solids* **23** (1975) 371.
23. F. WAKAI, S. SAKAGUCHI and Y. MATSUNO, *Adv. Ceram. Mats.* **1** (1986) 259.

Received 30 September 1987
and accepted 26 January 1988